



# Imaging manifestations of phosphaturic mesenchymal tumors: a description of two cases

Tianmin Tang<sup>1</sup>, Hongyu Jin<sup>2</sup>, Yujia Yang<sup>1</sup>

<sup>1</sup>Department of Ultrasound, West China Hospital, Sichuan University, Chengdu, China; <sup>2</sup>Department of Liver Surgery & Liver Transplantation, State Key Laboratory of Biotherapy and Cancer Center, West China Hospital, Sichuan University and Collaborative Innovation Center of Biotherapy, Chengdu, China

*Correspondence to:* Yujia Yang. Department of Medical Ultrasound, West China Hospital of Sichuan University, No. 37 Guoxue Alley, Chengdu 610041, China. Email: 441288637@qq.com.

Submitted Aug 08, 2022. Accepted for publication Feb 20, 2023. Published online Mar 06, 2023.

doi: 10.21037/qims-22-833

View this article at: <https://dx.doi.org/10.21037/qims-22-833>

## Introduction

Hypophosphatemic osteomalacia is a rare metabolic bone disease characterized by hypophosphatemia, increased urinary phosphate excretion, a low 25-hydroxyvitamin D level, and bone mineralization disorder (1). It has diverse etiologies, including X-linked hypophosphatemic rickets and autosomal dominant hypophosphatemic rickets (2). However, despite its rarity, hypophosphatemic osteomalacia can also be induced by a particular kind of neoplasm, which is referred to as tumor-induced osteomalacia (TIO).

TIO is an acquired metabolic bone disease. The clinical symptoms are progressive bone pain, myasthenia, and a limitation of motion. In serious cases, pathological fractures or pseudo-fractures may be observed. TIO results in excessive phosphate loss in the kidney due to an abnormal increase of phosphate-regulating factors secreted by the tumors (3). The tumors that lead to TIO are mostly benign and derive from the mesenchymal tissue of soft tissue or bone tissue. In 1991, Weidner summarized the pathological features of the tumor and named it a phosphaturic mesenchymal tumor (PMT) (4). PMT is a morphologically distinctive neoplasm that produces TIO, which usually occurs through the production of fibroblast growth factor 23 (FGF23) (5). FGF23, the regulator of phosphate, induces internalization of renal sodium/phosphate cotransporters, causing decreased tubular phosphate reabsorption. Moreover, FGF23 also inhibits the production of 1,25-dihydroxyl vitamin D [1,25-(OH)<sub>2</sub>D] (1,6). Pathologically, PMT is characterized by a highly unusual

admixture of bland spindle cells. These cells are a highly vascular stroma often appearing with microcystic change, a calcified matrix (sometimes resembling a chondroid or osteoid), osteoclast-like giant cells, and metaplastic bone (7).

PMTs are quite rare, with roughly only 450 cases having been reported thus far (8). PMTs, which are often located in bone or soft tissue in a concealed manner, are characterized by slow growth and an occult location, so they often lack obvious clinicopathological features. The diagnosis of PMT is often significantly delayed due to its rarity and vague symptoms, which include progressive bone pain, myopathies, arthralgias, fractures, and generalized weakness (9). Somatostatin receptor whole-body imaging is a targeted imaging method for screening suspected cases of TIO. However, the resolution of this technique is comparatively low, with a fraction of false-positive and false-negative cases occurring. Therefore, this examination is unsatisfactory for localizing tumors. <sup>68</sup>Ga tetraazacyclododecane-tetraacetic acid-DPhe1-Tyr3-octreotate (<sup>68</sup>Ga-DOTATATE) positron emission tomography/computed tomography (PET/CT) and <sup>18</sup>F-fluorodeoxyglucose (<sup>18</sup>F-FDG) PET/CT can also be used in the localization and qualitative diagnosis of tumors with greatly improved sensitivity and accuracy. Other than the techniques already mentioned, CT and magnetic resonance imaging (MRI) can clearly show the size and location of the lesions, as well as their anatomical relationships with the surrounding tissues. High-resolution MRI has the advantages of high soft-tissue resolution and multiple parameters, which provide additional evidence for



**Figure 1** A 55-year-old female with PMT. (A) T1-weighted magnetic resonance imaging showing a lobulated nodule with a clear edge in the subcutaneous tissue of the middle part of the right plantar pedis (arrow). (B) T2-weighted magnetic resonance imaging showing a lobulated nodule presented in the middle part of the right foot (arrow). PMT, phosphaturic mesenchymal tumor.

the diagnosis and localization of lesions. The resolution and quality of ultrasound images have improved because the equipment to perform ultrasonography has advanced. Considering the relatively reasonable cost and lack radiological harm, ultrasonography has become increasingly popular for both screening and diagnosing PMTs (10,11). In this report, the imaging manifestations of 2 cases diagnosed with PMT are carefully analyzed to provide an imaging pathway for the accurate diagnosis of PMT.

## Case presentation

### Case 1

A 55-year-old female presented with progressive bone and muscle pain in her chest wall and lower limbs concomitant with a mass in her right plantar pedis over the past 3 years. Three years ago, the patient accidentally found a soft tissue mass 1 cm × 3 cm in size in the right plantar pedis. The mass did not protrude from the skin surface and had no obvious tenderness or pain. Meanwhile, she had no symptoms, so the patient did not pay much attention to the mass. Two months after the discovery of the mass, the patient started to experience pain in many parts of the body. One year ago, due to the progressive aggravation of pain, the patient went to the local hospital and was diagnosed with osteoporosis according to CT. She was given supportive treatment, such

as calcium supplements, but she felt there was no obvious improvement after treatment.

Consequently, she came to West China Hospital, Sichuan University for further diagnosis and treatment. After admission, the physical examination indicated a soft tissue mass about 2 cm × 3 cm in size on the lateral side of the right plantar pedis. The mass protruded from the surface of the skin, had a clear boundary, and could be pushed around. The movement of the right hip joint was limited, while the movement of the left hip joint was fair. However, there was tenderness in multiple regions along the chest wall.

Laboratory examination of serum samples revealed a high level of parathyroid hormone of 9.99 pmol/L (normal range, 1.60–6.90 pmol/L), a low phosphate level of 0.70 mmol/L (normal range, 0.81–1.45 mmol/L), and a normal 25-hydroxyvitamin D and calcium level. Alkaline phosphatase was elevated and was noted to be 275 IU/L (normal range, 50–135 IU/L).

MRI showed a lobulated nodule about 22 mm × 18 mm in size with a clear boundary in the subcutaneous tissue of the middle part of the right plantar, which was T1 hypointense and T2 hyperintense. A small lesion of low T1 and high T2 signal intensity was observed under the articular surface of the right talus, and a weak signal ring was observed around it, which suggested osteochondral injury (Figure 1). Ultrasound examination showed a solid

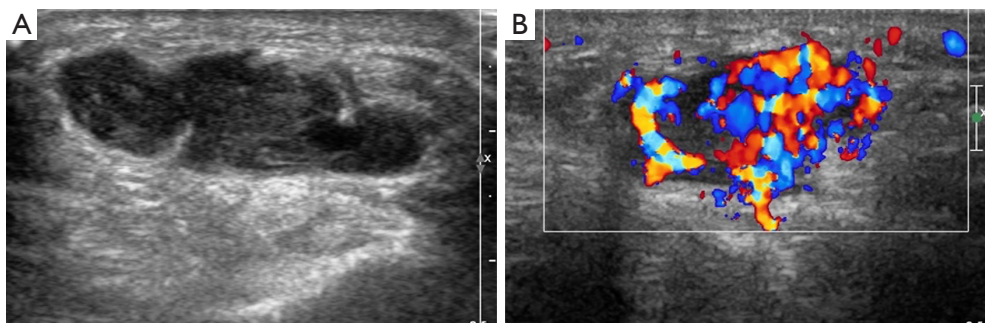


**Figure 2** Ultrasound images showing a solid lobulated hypoechoic mass. (A) B-mode ultrasound showing a solid oval hypoechoic mass with a well-defined boundary and an irregular shape in the middle of the right foot. (B) Color Doppler sonography image showing a rich blood flow signal in the mass.

lobulated hypoechoic mass in the middle of the right foot, which was about 29 mm × 21 mm × 21 mm in size, with a clear boundary and an irregular shape. Multiple spotty hyperechoic calcifications and small anechoic areas were found in the lesions (*Figure 2A*). The internal blood flow signals were abundant (*Figure 2B*). When these results were combined with blood biochemistry and urine electrolyte examinations, the mass was suspected to be PMT.

The patient underwent right plantar lesion excision biopsy and local fascial flap plasty under general anesthesia. The pathological results showed that the mass was a PMT in the right plantar pedis. Immunohistochemical features were as follows: CD56 (+); CD34 (-); PCK (-); SMA (-); DES (-); CD99 (-); D2-40 (-); NSE (-); Ki67 (MIB-1); and positive rate, 1–5%.

According to the biochemical examination, the inorganic phosphate level dramatically decreased to 0.55 mmol/L, and the calcium level reduced to 1.99 mmol/L within 1 hour after the surgery. The serum concentration of inorganic phosphate was 0.66 mmol/L, and the calcium level returned to normal (2.21 mmol/L) 1 day after the operation. The patient's laboratory testing of serum samples indicated that the inorganic phosphate level (0.91 mmol/L) and calcium level (2.18 mmol/L) returned to normal 2 days after surgery. There was no swelling or bleeding in the wound after the operation, and the patient felt relieved of the pain. During the 1-year follow-up through laboratory tests, the level of inorganic phosphate and calcium level remained normal. Furthermore, her limb movements were normal. She had no symptoms of pain during the 1-year follow-up.

## Case 2

A 36-year-old female patient was admitted to West China

Hospital, Sichuan University for “pain in both lower limbs with claudication for more than 3 years and difficulty walking for 2 years”. Three years ago, the patient had pain in both lower limbs when standing for a long time, mainly in both hips. Pain occurred during weight-bearing and activity and was alleviated after rest. Two years ago, the above symptoms of the patient gradually worsened, and it was difficult for the patient to walk.

Laboratory testing of serum samples revealed a high parathyroid hormone level of 8.53 pmol/L (normal range, 1.60–6.90 pmol/L), a low phosphate level of 0.20 mmol/L (normal range, 0.85–1.51 mmol/L), and normal 25-hydroxyvitamin D and calcium levels. Alkaline phosphatase was elevated and was noted to be 213 IU/L (normal range, 35–100 IU/L).

Dual-energy X-ray absorptiometry (DXA) showed that the absolute values of bone mineral density (BMD) of the L1, L2, L3, L4, L1–L4, femoral neck, and total hip were ( $\text{g}/\text{cm}^2$ ) 0.744, 0.691, 0.728, 0.794, 0.737, 0.512, and 0.437, respectively; the corresponding Z values were -1.7, -2.7, -2.8, -2.1, -2.4, -2.9, and -3.4, respectively.

PET/CT ( $^{18}\text{F}$ -FDG/ $^{68}\text{Ga}$ -DOTATATE) showed that the left palmar tubercle was associated with increased glucose metabolism and increased expression of the somatostatin receptor. It also indicated osteomalacia in multiple bilateral ribs and the pelvis with L5 double vertebral arch isthmus fractures (*Figure 3*).

MRI of the left foot showed a volar nodule of the first metatarsophalangeal joint, demonstrating an intermediate T1 signal with T2 hyperintensity (*Figure 3*). Ultrasound examination showed a heterogeneous hypoechoic oval mass 27 mm × 16 mm × 13 mm in size between the first and second metatarsophalangeal joints of the palm of the left foot with a clear boundary and a regular shape (*Figure 4A*).

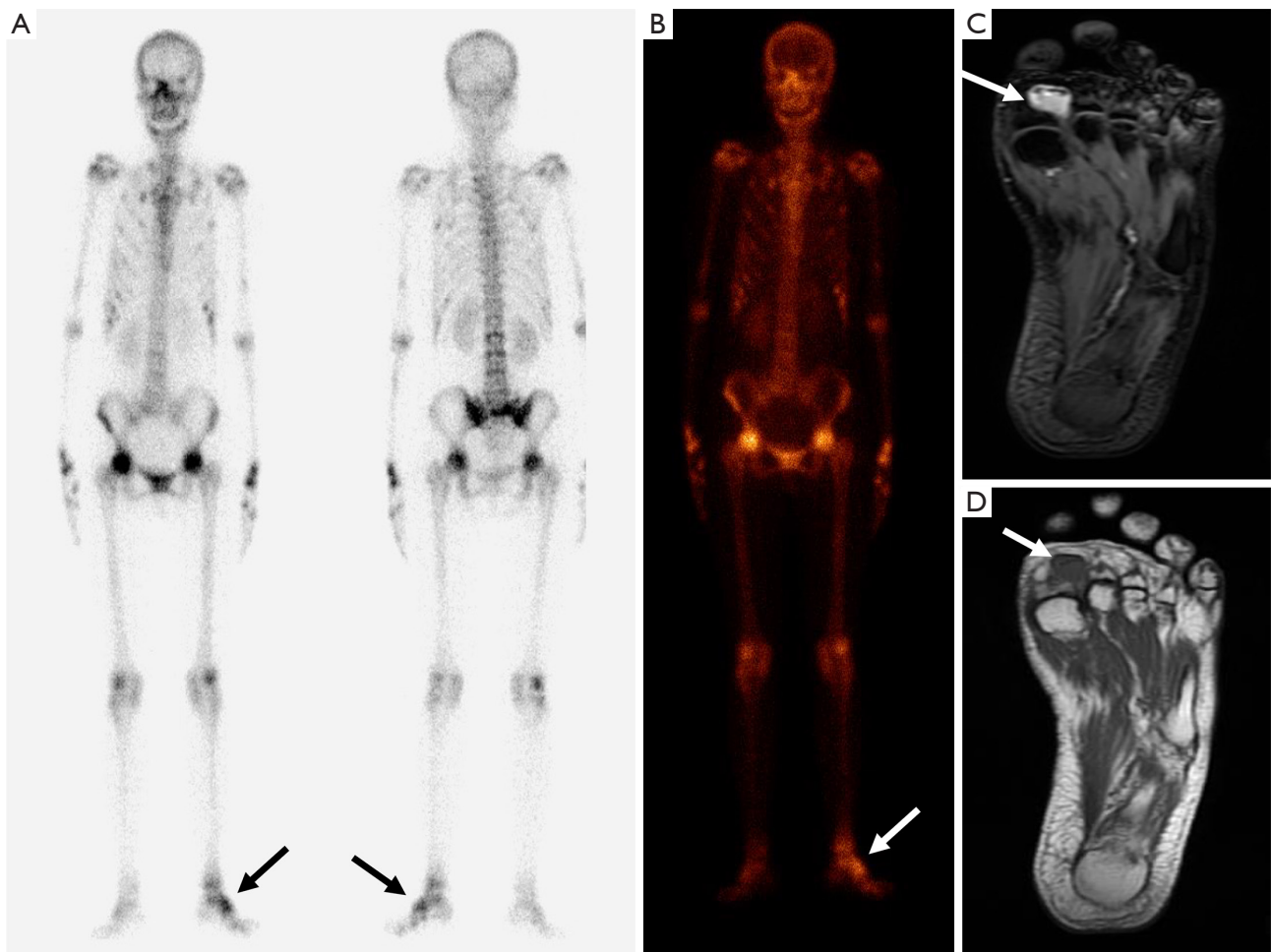


**Figure 3** A 36-year-old female with PMT. (A) A bone scan showing hypermetabolism of multiple bilateral ribs, lumbosacral vertebrae, bilateral sacroiliac joints, and bilateral femoral heads, especially of the left foot (arrows). (B) PET/CT showing the left palmar tubercle with increased glucose metabolism, increased expression of somatostatin receptor, and osteomalacia (arrow). (C,D) Magnetic resonance imaging showing a lobulated nodule between the first and second metatarsophalangeal joints of the palm of the left foot (arrows). PMT, phosphaturic mesenchymal tumor; PET/CT, positron emission tomography/computed tomography.

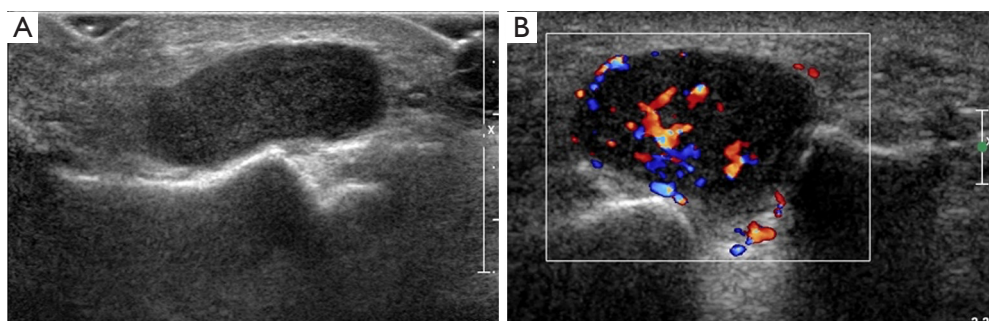


**Figure 4** Ultrasound examination showing a heterogeneous hypoechoic oval mass. (A) Ultrasonography showing a hypoechoic mass of the left foot. (B) The color Doppler sonography image of the mass showing a rich blood supply.

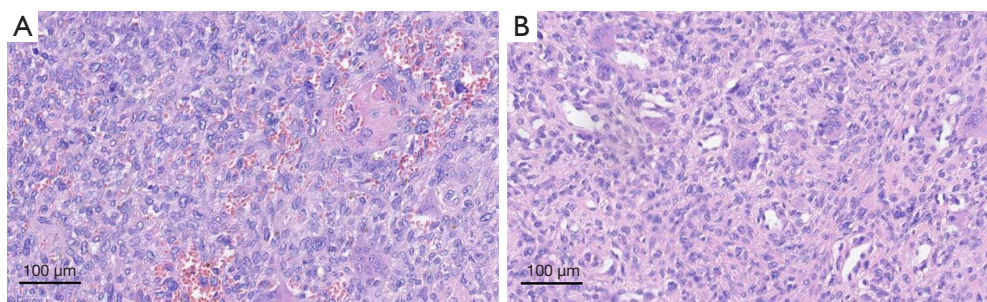


**Figure 5** A histologic image of a phosphaturic mesenchymal tumor. (A) Phosphaturic mesenchymal tumors typically consist of osteoclast-like giant cells and spindle cells and are associated with a basophilic matrix (HE,  $\times 100$ ). (B) The tumors typically contain numerous small capillaries (HE,  $\times 100$ ). HE, hematoxylin and eosin.

The mass was adjacent to the first and second metatarsal bones and the flexor digitorum tendon. A rich blood flow signal was detected in the mass (*Figure 4B*). These results, in combination with the patient's clinical history and blood biochemistry, suggested the presence of PMT.

The patient underwent surgical resection of the soft tissue mass in the left plantar pedis. Postoperative pathology showed that the lesions contained many osteoclast-like giant cells, accompanied by many fusiform, round, or polygonal cells. In the meantime, osteoid matrix, chondroid matrix, and mucoid matrix were found in the local region (*Figure 5*). Mitotic activity was observed [2–6/10 high-power field (HPF)]. Immunohistochemical features were as follows: SATB2 (+); CD56 (+); SSTR2 (+); ERG ( $\pm$ ); DOG-1 (-);  $\beta$ -C (-); STAT6 (-); P63 (-); S-100 (-); CD34 (-); EMA (-); and desmin (-). Taking into account the clinical manifestations, histopathological features, and imaging examination results, PMT was considered.

The inorganic phosphate level decreased to 0.18 mmol/L, and the calcium level was 2.04 mmol/L immediately after surgery. The level of inorganic phosphate was 0.37 mmol/L, and the calcium level returned to normal (2.20 mmol/L) within 1 day after surgery. The serum concentration of inorganic phosphate was 0.78 mmol/L 4 days after surgery. During the 2-year follow-up, the 25-hydroxyvitamin D level, parathyroid hormone level, and phosphate level remained normal.

All procedures performed in this study were conducted in accordance with the ethical standards of the institutional and/or national research committee(s) and with the Helsinki Declaration (as revised in 2013). Written informed consent was obtained from the patients to publish this case report and accompanying images. A copy of the written consent is available for review by the editorial office of this journal.

## Discussion

TIO, also known as oncogenic osteomalacia, is characterized by progressive bone pain and muscle weakness. In severe cases, osteoporosis and fractures may occur, which are usually found unintentionally or during a physical examination. As the disease progresses, PMT can occur anywhere in the body and is most likely found in the lower extremities, followed by the head and hip (12). Currently, the optimal treatment for PMT is surgical resection. In the 2 cases we described, both patients underwent surgical resection. After tumor resection, the patients' blood phosphate levels returned to normal in 2 days, and the pain was relieved to a large extent. It is worth noting that the blood phosphate level had a sudden decrease. It is suspected that the release of FGF23 from the tumor during the operation led to a sudden decrease in the phosphate level. However, the reason for the decrease in phosphate level still needs further study. Early and accurate diagnosis and identifying the location of the tumor are important for the treatment of PMT (9). However, the tumors are usually small in size and grow relatively slowly (13). Due to the lack of characteristic clinical manifestations in the early stage, the diagnosis of PMT is often delayed. The literature indicates that the average delay is about 5 years before the final diagnosis of PMT (14). Nonetheless, an accurate diagnosis could be made possible by the effective use of multiple modalities (15). Imaging examination combined with laboratory tests could be effective in confirming the diagnosis.

The biochemical characteristics of PMT are decreased phosphate levels, increased 24-hour urinary phosphate excretion, increased alkaline phosphatase, and normal or decreased calcium. Some cases can be accompanied by

secondary hyperparathyroidism (16). Therefore, serology examination is particularly important, which is the first step to inferring PMT, and it is important that a low phosphate value not be ignored. PMT secretes FGF23, inhibiting the absorption of phosphate in the intestine and renal tubules, promoting the excretion of urinary phosphate, and causing hypophosphatemia. Meanwhile, FGF23 can inhibit the activity of 25-(OH)D 1- $\alpha$  hydroxylase and reduce the production of 1,25-(OH)<sub>2</sub>D. These processes result in osteomalacia (12,17). Thus, phosphate, alkaline phosphatase, calcium, parathyroid hormone, and vitamin D metabolites [25-hydroxyvitamin D and 1,25-(OH)<sub>2</sub>D] should be measured. Furthermore, the measurement of serum FGF23 can assist in the diagnosis of PMT. An obviously high level of FGF23 in the serum from a specific vein strongly suggests the presence of an FGF23-producing tumor in the region distal to the sampling point and helps establish the diagnosis of TIO (18,19).

Imaging examinations have important clinical value in the diagnosis and postoperative follow-up of PMT. Tumors should be identified through a stepwise approach, including functional imaging, and the identification should be confirmed with anatomic imaging, such as CT, MRI, or ultrasound (20). The imaging features of PMT are as follows: A unique feature best demonstrated on CT is the presence of the internal matrix, which is likely correlated with matrix calcification. In an MRI examination, the majority of lesions demonstrate an intermediate T1 signal with T2 hyperintensity. The characteristic feature of a PMT on PET/CT is metabolically active neoplasms (8,21,22). Ultrasound examination can determine the size, boundary, echo, and blood flow signal of PMT lesions. The ultrasound findings of PMT are a solid hypoechoic tumor structure with a heterogeneous internal echo. The heterogeneous hyperechoic echo corresponds to the unique calcium deposition in the pathology of the PMT, while the anechoic structure corresponds to the cyst in the pathology of the PMT. Color Doppler flow imaging shows abundant blood flow, which corresponds to many abnormal blood vessels of PMT in the pathological examination. CT has advantages for bone imaging, but it uses radiation, which cannot be used repeatedly during the follow-up of patients. MRI has the highest soft tissue resolution, but is less economically viable for price for patients. Ultrasound examination provides images in real-time, requires no radiation, and is inexpensive. However, it is weak in detecting deep positions, meaning some lesions cannot be detected and identified clearly. Therefore, the multiple

image modality should be applied to diagnose and identify PMTs.

In this study, we described 2 cases that had clinical, biochemical, and imaging evidence of PMT. When the doctor found a mass on the surface of 2 patients, an imaging examination was performed for each patient. Therefore, this kind of solid tumor can be identified as a PMT based on the hypoechoic imaging manifestations, rich blood supply, and intermediate T1 signal with T2 hyperintensity, combined with the patient's symptoms, low phosphate level, and high FGF23 level. A combination of laboratory tests and imaging examinations could provide a precise diagnosis of PMT. The image characteristics of PMT are extremely helpful in diagnosing and localizing a PMT. These characteristics include the heterogeneous hypoechoic solid structure, rich blood flow, the presence of an anechoic cyst and hyperechoic calcification on ultrasonography, the presence of an internal matrix in CT, and the intermediate T1 signal with T2 hyperintensity in MRI.

## Acknowledgments

*Funding:* None.

## Footnote

*Conflicts of Interest:* All authors have completed the ICMJE uniform disclosure form (available at <https://qims.amegroups.com/article/view/10.21037/qims-22-833/coif>). The authors have no conflicts of interest to declare.

*Ethical Statement:* The authors are accountable for all aspects of the work in ensuring that questions related to the accuracy or integrity of any part of the work are appropriately investigated and resolved. All procedures performed in this study were conducted in accordance with the ethical standards of the institutional and/or national research committee(s) and with the Helsinki Declaration (as revised in 2013). Written informed consent was obtained from the patients to publish this case report and accompanying images. A copy of the written consent is available for review by the editorial office of this journal.

*Open Access Statement:* This is an Open Access article distributed in accordance with the Creative Commons Attribution-NonCommercial-NoDerivs 4.0 International License (CC BY-NC-ND 4.0), which permits the non-

commercial replication and distribution of the article with the strict proviso that no changes or edits are made and the original work is properly cited (including links to both the formal publication through the relevant DOI and the license). See: <https://creativecommons.org/licenses/by-nc-nd/4.0/>.

## References

- Boland JM, Tebben PJ, Folpe AL. Phosphaturic mesenchymal tumors: what an endocrinologist should know. *J Endocrinol Invest* 2018;41:1173-84.
- Arai R, Onodera T, Terkawi MA, Mitsuhashi T, Kondo E, Iwasaki N. A rare case of multiple phosphaturic mesenchymal tumors along a tendon sheath inducing osteomalacia. *BMC Musculoskelet Disord* 2017;18:79.
- Folpe AL, Fanburg-Smith JC, Billings SD, Bisceglia M, Bertoni F, Cho JY, et al. Most osteomalacia-associated mesenchymal tumors are a single histopathologic entity: an analysis of 32 cases and a comprehensive review of the literature. *Am J Surg Pathol* 2004;28:1-30.
- Weidner N. Review and update: oncogenic osteomalacia-rickets. *Ultrastruct Pathol* 1991;15:317-33.
- Jo VY, Fletcher CD. WHO classification of soft tissue tumours: an update based on the 2013 (4th) edition. *Pathology* 2014;46:95-104.
- Florenzano P, Hartley IR, Jimenez M, Roszko K, Gafni RI, Collins MT. Tumor-Induced Osteomalacia. *Calcif Tissue Int* 2021;108:128-42.
- Weidner N, Santa Cruz D. Phosphaturic mesenchymal tumors. A polymorphous group causing osteomalacia or rickets. *Cancer* 1987;59:1442-54.
- Folpe AL. Phosphaturic mesenchymal tumors: A review and update. *Semin Diagn Pathol* 2019;36:260-8.
- Richardson AL, Richardson OK. Phosphaturic mesenchymal tumor: Case report. *Radiol Case Rep* 2019;14:1518-24.
- Busquet F, Gahier-Penhoat M, Lescour V, Maugars Y, Guillot P. Contribution of ultrasound to diagnosing a phosphaturic mesenchymal tumor. *Joint Bone Spine* 2018;85:639-40.
- Jones O, Murphy SH, Poole KES, Watkins AJ, Durrani AJ. Phosphaturic Mesenchymal Tumor of the Ankle: A Case Report and Review of the Literature. *J Foot Ankle Surg* 2022;61:185-8.
- Jiang Y, Xia WB, Xing XP, Silva BC, Li M, Wang O, Zhang HB, Li F, Jing HL, Zhong DR, Jin J, Gao P, Zhou L, Qi F, Yu W, Bilezikian JP, Meng XW. Tumor-induced osteomalacia: an important cause of adult-onset hypophosphatemic osteomalacia in China: Report of 39 cases and review of the literature. *J Bone Miner Res* 2012;27:1967-75.
- Shiba E, Matsuyama A, Shibuya R, Yabuki K, Harada H, Nakamoto M, Kasai T, Hisaoka M. Immunohistochemical and molecular detection of the expression of FGF23 in phosphaturic mesenchymal tumors including the non-phosphaturic variant. *Diagn Pathol* 2016;11:26.
- Komínek P, Stárek I, Geierová M, Matoušek P, Zeleník K. Phosphaturic mesenchymal tumour of the sinonasal area: case report and review of the literature. *Head Neck Oncol* 2011;3:16.
- Kawai S, Ariyasu H, Furukawa Y, Yamamoto R, Uraki S, Takeshima K, Warigaya K, Nakamoto Y, Akamizu T. Effective localization in tumor-induced osteomalacia using (68)Ga-DOTATOC-PET/CT, venous sampling and 3T-MRI. *Endocrinol Diabetes Metab Case Rep* 2017.
- Kurien R, Rupa V, Thomas M. Varied presentation of sinonasal phosphaturic mesenchymal tumour: report of a case series with follow-up. *Eur Arch Otorhinolaryngol* 2019;276:1677-84.
- Angeles-Angeles A, Reza-Albarrán A, Chable-Montero F, Cordova-Ramón JC, Albores-Saavedra J, Martínez-Benitez B. Phosphaturic mesenchymal tumors. Survey of 8 cases from a single Mexican medical institution. *Ann Diagn Pathol* 2015;19:375-80.
- Takeuchi Y, Suzuki H, Ogura S, Imai R, Yamazaki Y, Yamashita T, Miyamoto Y, Okazaki H, Nakamura K, Nakahara K, Fukumoto S, Fujita T. Venous sampling for fibroblast growth factor-23 confirms preoperative diagnosis of tumor-induced osteomalacia. *J Clin Endocrinol Metab* 2004;89:3979-82.
- Andreopoulou P, Dumitrescu CE, Kelly MH, Brillante BA, Cutler Peck CM, Wodajo FM, Chang R, Collins MT. Selective venous catheterization for the localization of phosphaturic mesenchymal tumors. *J Bone Miner Res* 2011;26:1295-302.
- Feng J, Jiang Y, Wang O, Li M, Xing X, Huo L, Li F, Yu W, Zhong DR, Jin J, Liu Y, Qi F, Lv W, Zhou L, Meng XW, Xia WB. The diagnostic dilemma of tumor induced osteomalacia: a retrospective analysis of 144 cases. *Endocr J* 2017;64:675-83.
- Broski SM, Folpe AL, Wenger DE. Imaging features of phosphaturic mesenchymal tumors. *Skeletal Radiol* 2019;48:119-27.
- Singh D, Chopra A, Ravina M, Kongara S, Bhatia E,

Kumar N, Gupta S, Yadav S, Dabadghao P, Yadav R, Dube V, Kumar U, Dixit M, Gambhir S. Oncogenic osteomalacia: role of Ga-68 DOTANOC PET/CT scan

in identifying the culprit lesion and its management. *Br J Radiol* 2017;90:20160811.

**Cite this article as:** Tang T, Jin H, Yang Y. Imaging manifestations of phosphaturic mesenchymal tumors: a description of two cases. *Quant Imaging Med Surg* 2023;13(5):3343-3350. doi: 10.21037/qims-22-833